THE JOURNAL OF PHYSICAL CHEMISTRY B

Article

pubs.acs.org/JPCB

# Initial Excited-State Structural Dynamics of Thymine Derivatives

Brant E. Billinghurst,[†] Sulayman A. Oladepo,[‡] and Glen R. Loppnow*

Department of Chemistry, University of Alberta, Edmonton, Alberta, T6G 2G2, Canada

**ABSTRACT:** Thymine is one of the pyrimidine nucleobases found in DNA. Upon absorption of UV light, thymine forms a number of photoproducts, including the cyclobutyl photodimer, the pyrimidine pyrimidinone [6–4] photoproduct and the photohydrate. Here, we use UV resonance Raman spectroscopy to measure the initial excited-state structural dynamics of the $N_1$-substituted thymine derivatives $N_1$-methylthymine, thymidine, and thymidine 5′-monophosphate in an effort to understand the role of the N1 substituent in determining the excited-state structural dynamics and the subsequent photochemistry. The UV resonance Raman spectrum of thymidine and thymidine 5′-monophosphate are similar to that of thymine, suggesting that large masses at $N_1$ effectively isolate the vibrations of the nucleobase. However, the UV resonance Raman spectrum of $N_1$-methylthymine is significantly different, suggesting that the methyl group couples into the thymine ring vibrations. The resulting resonance Raman intensities and absorption spectra are self-consistently simulated with a time-dependent expression to quantitatively extract the initial excited-state slopes, homogeneous and inhomogeneous linewidths, and electronic parameters. These results are discussed in the context of the known photochemistry of thymine and its derivatives.

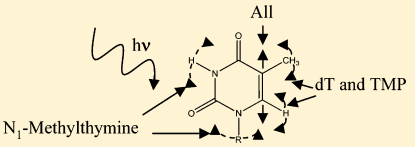


## INTRODUCTION

Deoxyribonucleic acid (DNA), which stores genetic information, and ribonucleic acid (RNA), which mediates translation of the genetic code into proteins, are composed of two purines, adenine and guanine, and three pyrimidines, cytosine, thymine, and uracil.[1] Thymine (Scheme 1) is only present in DNA, while uracil is present only in RNA, with very few exceptions. Interest in thymine arises from the fact that it is the most photochemically active nucleobase in DNA.[2] Thymine dinucleotides (TpT) preferentially form the cyclobutane pyrimidine dimer (CPD) with a quantum yield, $\phi$, of 0.013 as a result of [2π+2π]-cycloaddition between the C═C bonds of adjacent thymines or the [6–4] photoproduct ($\phi$ = 0.003) as a result of [2π+2π]-cycloaddition between the C═C bond of one thymine and the C═O bond of the adjacent thymine (Scheme 2).[2]

**Scheme 1**

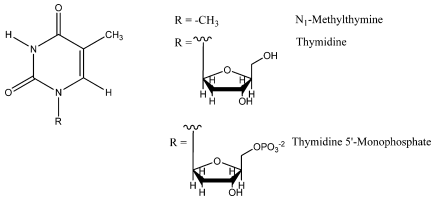


A probe of the initial excited-state structural dynamics is crucial to understanding the photochemistry of the nucleobases, because evolution on the excited-state potential energy surface is the first step of the photochemical reaction after absorption. Resonance Raman spectroscopy is a powerful probe of the initial excited-state structural dynamics.[3,4] By tuning the laser's excitation wavelength into the absorption band of interest, resonant enhancement occurs for those vibrational modes coupled to the electronic transition. For these modes, the resonance Raman band intensity is directly proportional to the slope of the excited-state potential energy surface along that vibrational coordinate. Thus, the intensities of the resonance Raman bands will directly reflect the excited-state forces acting on the molecule along each normal coordinate.[3,4]

There have been many UV resonance Raman studies of nucleic acid components, including thymine and its derivatives.[5−11] Spiro, et al.[12] were the first to measure thymidine monophosphate (TMP) resonance Raman excitation profiles. While the UV resonance Raman excitation profiles of TMP were determined in that study and supported by CINDO calculations, the main goal of the work was to determine the nature of the excited electronic state, not to determine the initial excited-state structural dynamics. Furthermore, the CINDO calculations had no experimental basis to validate their accuracy. More recently, partial resonance Raman excitation profiles and resulting initial excited-state structural dynamics have been determined for thymidine by Zhu, et al.[13] They postulated that the deoxyribosyl sugar vibrations lower the barrier between the Franck−Condon region and the conical intersection that leads to internal conversion, primarily by flattening the excited-state potential energy surface, leading to a faster observed excited-state lifetime in thymidine than thymine.[14−21] No mention is

**Scheme 2**

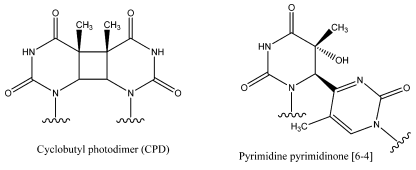


**Special Issue:** Richard A. Mathies Festschrift

**Received:** February 28, 2012
**Revised:** May 26, 2012
**Published:** June 14, 2012

made of the intersystem crossing rate, which has recently been shown to be important in CPD formation of isolated thymine derivatives.[22,23]

Previous analysis of the resonance Raman excitation profiles and absorption spectra for thymine,[24] uracil,[25] and uracil derivatives[26,27] within the 266 nm absorption band showed that their excited-state structural dynamics lie along primarily C5=C6 bond lengthening and C5, C6 pyramidalization coordinates. The resonance Raman-derived initial excited-state structural dynamics are consistent with both transient IR spectra,[28] which shows that the thymine CPD photoproduct forms in less than 1 ps, and computations,[29] which show that the expected thymine CPD transition state structure has a longer C5C6 bond length and more $sp^3$-like pyramidalization of the C5 and C6 carbon atoms. From this data, it was postulated[22−25] that the methyl group in thymine acts as a mass barrier and localizes the reorganization energy along bond-lengthening coordinates. In addition to these two coordinates, the mode analysis indicated that significant motion also occurs along N1H and C6H12 bending motions.

In order to provide a clearer picture of the role of N1-substituents on the initial excited-state structural dynamics of thymine derivatives, we here report complete resonance Raman excitation profiles and the resulting initial mode-dependent, excited-state slopes for three thymine derivatives, $N_1$-methylthymine (1-MeT), thymidine (Thd), and thymidine-5′-monophosphate (TMP). The results show that large masses, e.g., a sugar or sugar monophosphate, at N1 vibrationally decouple the nucleobase chromophore from the N1 substituent, but a smaller methyl group is coupled vibrationally to the nucleobase. In all cases, the N1-substituent increases both the homogeneous and inhomogeneous linewidths, indicating stronger solvent−solute interactions on a variety of time scales. These greater homogeneous and inhomogeneous linewidths may be responsible for the observed N1-dependent excited-state lifetimes in thymine derivatives.[18,19]

## EXPERIMENTAL SECTION

1-MeT (99%, Sigma, Oakville, Ontario), Thd (99%, Sigma, Oakville, Ontario), TMP (99%, Sigma, Oakville, Ontario), and sodium sulfate (99%, EMD Chemicals Inc., Gibbstown, NJ) were obtained commercially and used without further purification. All samples were prepared using nanopure water from a Barnstead water filtration system (Boston, MA).

Laser excitation for the resonance Raman experiments was obtained by using a picosecond mode-locked Ti:sapphire laser (Coherent, Santa Clara, CA) pumped with a Verdi V-10 diode-pumped laser (Coherent, Santa Clara, CA). In order to obtain the 233, 250, 266, 275, and 290 nm wavelengths, the output of the Ti:sapphire was doubled using a lithium triborate (LBO) crystal followed by third harmonic generation in a $\beta$-barium borate ($\beta$-BBO) crystal (Inrad Model 5−050, Northvale, NJ). Typical laser powers were 6−30 mW. The resulting laser beam was spherically focused on an open stream of flowing solution in a 135°-backscattering geometry. All the resonance Raman spectra were obtained using solutions with sample concentrations of 1−2 mM and containing 0.4 M sodium sulfate internal standard. The addition of sodium sulfate as an internal standard had no noticeable effect on either the absorption or resonance Raman spectra of any of the samples. The resonance Raman scattering was focused into a double-grating spectrophotometer with a diode array detector. For all three compounds, measurements of the resonance Raman spectra and determinations of intensities were repeated on three fresh samples at each wavelength. Frequency calibration was performed by measuring the Raman scattering of organic solvents for which the peak positions are known (n-pentane, cyclohexane, dimethylformamide, ethanol, acetonitrile and acetic acid). Frequencies are accurate to ±2 $cm^{-1}$. Analysis of the data was performed as previously described.[30] Absorption spectra were acquired before and after each Raman scan using a diode array spectrometer (Hewlett-Packard, model 8452A, Sunnyvale, CA). No significant change in absorbance was observed, suggesting that a bulk photoalteration parameter below 5% was observed.[31]

The methods used for converting the resonance Raman intensities of the three thymine derivatives into absolute cross sections and for self-absorption correction have been described previously.[32−34] The experimental differential Raman cross sections for sulfate used in this work were $4.11 \times 10^{-12}$, $2.85 \times 10^{-12}$, $2.08 \times 10^{-12}$, $1.77 \times 10^{-12}$, and $1.35 \times 10^{-12}$ $Å^2$/molecule·sr at 233, 250, 266, 275, and 290 nm, respectively. Depolarization ratios of 0.33 and 0.05 were used for the thymine derivatives and sulfate, respectively.

The 260 nm-excited resonance Raman spectrum of 1-MeT, Thd, and TMP in the overtone and combination band region was recorded using the same system as described for the fundamental region, except 1.17 M hydracrylonitrile was used as an internal standard. The Raman cross-section of the 2260 $cm^{-1}$ hydracrylonitrile band was determined by referencing it to the 1654 $cm^{-1}$ peak of Thd. Hydracrylonitrile had no effect on the absorption or resonance Raman spectra.

## THEORY

The resonance Raman excitation profiles were simulated with the time-dependent wavepacket formalism expressed by the following equations:[35]

$$\sigma_R(E_L) = \frac{8\pi E_S^3 E_L e^4 M^4}{9\hbar^6 c^4} \int_0^\infty dE_0 H(E_0) \times \left| \int_0^\infty dt \langle f|i(t)\rangle \exp\left\{\frac{i(E_L + \varepsilon_i)t}{\hbar}\right\} G(t) \right|^2 \quad (1)$$

$$\sigma_A(E_L) = \frac{4\pi E_L e^2 M^2}{6\hbar^2 cn} \int_0^\infty dE_0 H(E_0) \int_{-\infty}^\infty dt \langle i|i(t)\rangle \times \exp\left\{\frac{i(E_L + \varepsilon_i)t}{\hbar}\right\} G(t) \quad (2)$$

where $E_L$ and $E_S$ are the energies of the incident and scattered photons, respectively, $M$ is the transition length, $n$ is the refractive index, $\varepsilon_i$ is the energy of the initial vibrational state, $H(E_0)$ is a normalized inhomogeneous distribution of zero−zero energies around an average energy ($\bar{E}_0$) expressed as

$$H(E_0) = (2\pi\theta)^{-1/2} \exp\left\{\frac{-(\bar{E}_0 - E_0)^2}{2\theta^2}\right\} \quad (3)$$

where $\theta$ is the standard deviation of the distribution, $|i\rangle$ and $|f\rangle$ are the initial and final vibrational wave functions in the Raman process, $|i(t)\rangle$ is the initial ground-state vibrational wave function propagated on the excited-state potential energy surface, and $G(t)$ is the homogeneous line width function. Within the separable harmonic oscillator approximation, the $\langle i|i(t)\rangle$ and $\langle f|i(t)\rangle$ overlaps are significantly sensitive only to the differences


dx.doi.org/10.1021/jp301952v | J. Phys. Chem. B 2012, 116, 10496−10503

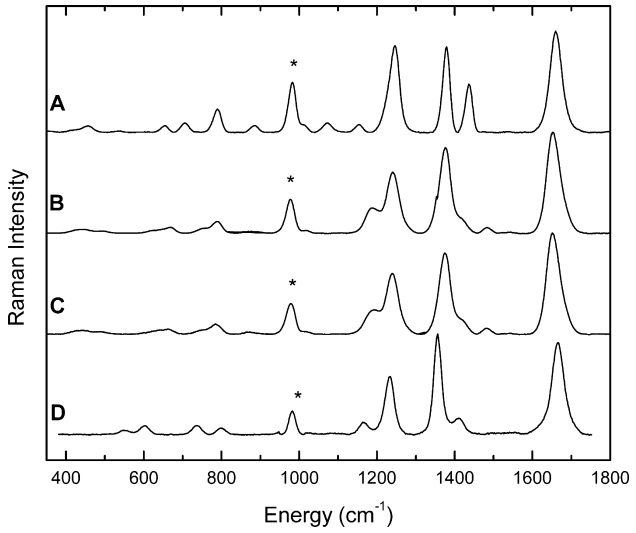


**Figure 1.** Resonance Raman spectra of 1 mM 1-MeT (A), 1 mM TMP (B), 1 mM Thd (C), and 3 mM thymine (D) in water excited at 266 nm. The bands due to the internal standards (0.4 M sodium sulfate) are indicated by asterisks (*).

**Table 1. Raman Frequencies, Assignments, and Harmonic Parameters for 1-MeT**

| mode[a] ($cm^{-1}$) | assignment[b] | $\|\Delta\|$[c] | $E$[d] ($cm^{-1}$) |
|---|---|---|---|
| 1673 | $\nu(C_5C_6)$ [58] | 0.67 | 375.5 |
| 1473 | be($N_1$Me) | 0.35 | 90.2 |
| 1379 | be($N_3H_9$) [42], be($C_6H_{12}$) [19] | 0.45 | 139.6 |
| 1242 | $\nu(C_2N_3)$ [30], be(ring) [17], $\nu(C_5C_{11})$ [13] | 0.55 | 187.9 |
| 1158 | $\nu(N_3C_4)$ [27], $\nu(C_5C_{11})$ [14], $\nu(C_2N_3)$ [13] | 0.13 | 9.8 |
| 1079 | be ($N_1$Me) [42], $\nu(C_6N_1)$ [14], $\nu(N_1Me)$ [13] | 0.13 | 9.1 |
| 885 | $\nu(N_1C_2)$ [25], $\nu(C_5C_{11})$ [14], $\nu(N_1Me)$ [13] | 0.11 | 5.3 |
| 789 | be(ring) [41], $\nu(C_5C_6)$ [16] | 0.22 | 19.0 |
| 702 | be(ring) [51], $\nu(C_5C_{11})$ [11] $\nu(N_1Me)$ [11] | 0.17 | 10.1 |
| 651 | $\gamma(N_3H)$ [90], $\tau$(ring) [10] | 0.10 | 3.3 |
| 447 | be(ring) [79] | 0.12 | 3.2 |

[a]Frequencies listed are the experimental frequencies reported here. [b]Abbreviations: $\nu$ is stretching, $\gamma$ is out-of-plane bending, and be is in-plane bending. The numbers represent the percentage of that internal coordinate in the mode. Assignments are from ref 39. Only the internal coordinates with percentages larger than 10% are listed. [c]Displacements ($\Delta$) are in units of dimensionless normal coordinates and were obtained by fitting eqs 1 and 2 with the following parameters: temperature $T$ = 298 K, Brownian oscillator line shape $\kappa = \Lambda/D$ = 0.1, Gaussian homogeneous line width $\Gamma_G$ = 900 $cm^{-1}$, inhomogeneous line width $\Theta$ = 1100 $cm^{-1}$, zero−zero energy $E_o$ = 35 500 $cm^{-1}$ and transition length $M$ = 0.66 Å. The estimated errors in the parameters used in the calculation are as follows: $E_o$ ± 1%, $M$ ± 1%, $\Gamma$ ± 5%, $\Delta$ ± 5%, and $\Theta$ ± 5%. [d]$E$ is the reorganization energy calculated using $E = \Delta^2\omega/2$.

in ground and excited−state equilibrium geometries along each normal mode ($\Delta$). Thus, the resonance Raman intensities directly reflect the dynamics of the excited-state.

For molecules interacting with a bath, $G(t)$ represents the dynamics of the chromophore-solvent coupling. The solute−solvent interactions that contribute to the solvent-induced homogeneous broadening are modeled using the Brownian oscillator model developed by Mukamel and co-workers.[36] The general implementation of these equations for absorption and resonance Raman spectroscopy have been described in detail

**Table 2. Raman Frequencies, Assignments, and Harmonic Parameters for Thd**

| mode[a] ($cm^{-1}$) | assignment[b] | $\|\Delta\|$[c] | $E$[d] ($cm^{-1}$) |
|---|---|---|---|
| 1654 | $\nu(C_5C_6)$ [61], be($C_6H$) [13], $\nu(C_6N1)$ [−8], $\nu(C_5Me)$ [−5] | 0.70 | 405.2 |
| 1413 | $\nu(C_2N_3)$ [15], $\nu(C_4C_5)$ [13], $CH_3$ umb [11], $\delta(N_1H)$ [9], $\nu(N_1C_2)$ [−8], be($C_4O$) [7], be($C_2O$) [7], ring $\delta$ 2 [−6], be($N_3H$) [−6] | 0.24 | 40.7 |
| 1374 | be($C_6H$) [42], $\nu(C_5C_6)$ [12], $\nu(N_1C_2)$ [9], $\nu(C_2N_3)$ [−9] | 0.58 | 231.1 |
| 1240 | $\nu(C_5Me)$ [29], $\nu(C_6N1)$ [−21], ring $\delta$ 1 [12], $\nu(N_1C_2)$ [10], $\nu(C_4C_5)$ [−10], $\nu(C_2N_3)$ [−8] | 0.57 | 201.4 |
| 1189 | $\nu(C_2N_3)$ [21], be($C_6H_{12}$) [20], be($N_1H_7$) [−16], $\nu(N_3C_4)$ [−12], $\nu(C_6N_1)$ [−11] | 0.36 | 77.0 |
| 780 | $\gamma(C_2O_8)$ [60], ring $\delta$ 6 [−12], ring $\delta$ 4 [8], $\gamma(C_4O_{10})$ [6], $\gamma(N_3H_9)$ [−5] | 0.32 | 39.9 |
| 439 | ring $\delta$ 6 [32], $\gamma(N_1H)$ [−17], $\gamma(C_5H)$ [−17], ring $\delta$ 4 [16], ring $\delta$ 5 [−9], $\gamma(C_4O)$ [−7] | 0.27 | 16.0 |

[a]Frequencies listed are the experimental frequencies reported here. [b]Abbreviations: $\nu$ is stretching, $\delta$ is deformation, $\gamma$ is out-of-plane bending, umb is umbrella, and be is in-plane bending. The numbers represent the percentage of that internal coordinate in the mode. Assignments are from ref 8. Only the internal coordinates with percentages of 5% or larger are listed. [c]Displacements ($\Delta$) are in units of dimensionless normal coordinates and were obtained by fitting eqs 1 and 2 with the following parameters: temperature $T$ = 298 K, Brownian oscillator line shape $\kappa = \Lambda/D$ = 0.1, Gaussian homogeneous line width $\Gamma_G$ = 1150 $cm^{-1}$, inhomogeneous line width $\Theta$ = 1320 $cm^{-1}$, zero−zero energy $E_o$ = 35850 $cm^{-1}$, and transition length $M$ = 0.79 Å. The estimated errors in the parameters used in the calculation are as follows: $E_o$ ± 1%, $M$ ± 1%, $\Gamma$ ± 5%, $\Theta$ ± 5%, and $\Delta$ ± 5%. [d]$E$ is the reorganization energy calculated using $E = \Delta^2\omega/2$.

previously.[3,4,24−27,30,32−34,37,38] In our analysis we assume that the system remains within the strongly damped and high temperature ($\hbar\Lambda \ll kT$) limits.

The initial guesses for the $\Delta$'s along each normal coordinate were based on the assumption that the average relative resonance Raman intensities are proportional to $\Delta^2$, with the intensity of the ca. 1670 $cm^{-1}$ mode arbitrarily set to 1. The relative $\Delta$'s were scaled to reproduce the experimentally observed absorption and resonance Raman excitation profile bandwidths. All observed fundamental modes for each thymine derivative were included in each time-dependent calculation. The ca. 2600 $cm^{-1}$ combination mode was further used to constrain the simulation. All other parameters were selected to give good agreement between the simulated and experimental absorption spectrum and resonance Raman excitation profiles. The parameters were then optimized iteratively as described previously[3,4,24−27,30,32−34,37,38] until the best possible agreement was obtained for the calculated and experimental absorption spectrum and resonance Raman excitation profiles.

## RESULTS

The resonance Raman spectra of thymine, 1-MeT, Thd, and TMP are shown in Figure 1. The spectra of Thd and TMP are both very similar to the spectrum of thymine. The spectrum of TMP is also similar to that reported previously.[12] Due to the similarities between the spectra of Thd, TMP, and thymine, the assignments for the peaks observed for both Thd and TMP (Tables 1 and 2) have been based on the potential energy distribution given for thymine.[8] The spectrum of 1-MeT differs from those of the other thymine derivatives presented here. Assignments for the 1-MeT peaks (Table 1) were based on

calculations by Morzyk-Ociapa, et al.[39] using the DFT(BLYP) method and D95 V** basis set.

It can be seen by comparing all of the spectra in Figure 1 that all spectra have three peaks in common: the ~1673 $cm^{-1}$ band, which is assigned to the C5═C6 stretch, the ~1373 $cm^{-1}$ band, which is assigned to C6H and N3H bending mode, and the ~1243 $cm^{-1}$ band, which is either assigned to the C2−N3 stretch, ring bend, and C5−C11 stretch for 1-MeT, or to the C5−C11 stretch, ring stretch, and C6H deformation for the other thymine derivatives (Table 1). The resonance Raman spectra of Thd and TMP are similar to that of thymine, and differ from thymine only in the weak peaks observed between 500 and 900 $cm^{-1}$ and an additional weak peak at ~1480 $cm^{-1}$ in Thd and TMP. This latter peak is assigned to a methyl scissoring mode; however, this peak does not appear at excitation wavelengths above 266 nm and is not considered here further. 1-MeT bears little resemblance to the other spectra other than three peaks that have been previously noted. This suggests that the methyl group on $N_1$ in 1-MeT has stronger vibrational coupling to the rest of the pyrimidine base than either the deoxyribose or deoxyribose-5′-phosphate.

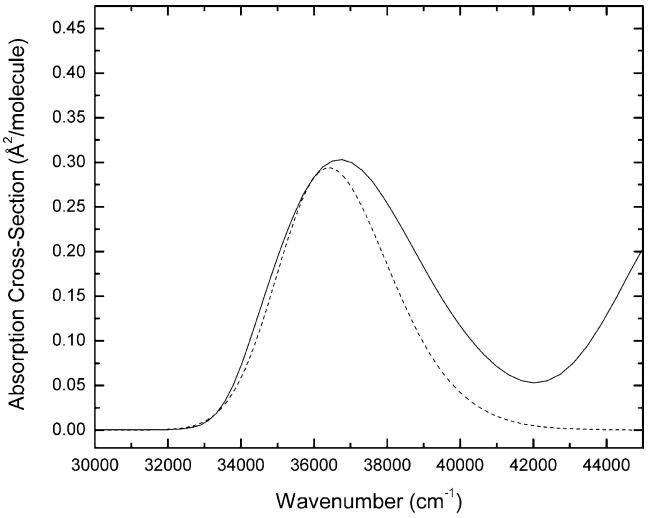


**Figure 2.** Experimental (solid line) and simulated (dotted line) absorption spectra of 1-MeT. The simulated absorption spectrum was calculated using eq 2 with the parameters in Table 1. Discrepancies observed above 38000 $cm^{-1}$ are due to higher energy electronic transitions which were not modeled here.

The experimental and simulated absorption spectra for 1-MeT, Thd, and TMP are shown in Figures 2, 4, and 6 while the experimental and simulated resonance Raman profiles are shown in Figures 3, 5, and 7, respectively. In general, Figures 2−7 show good agreement between the experimental and calculated resonance Raman profiles and absorption spectra. Deviations between the experimental and calculated absorption spectra (Figures 2, 4, and 6), which appear above 38000 $cm^{-1}$, are attributed to higher energy electronic transitions, which are not modeled here.

For 1-MeT, a number of deviations can also be observed in the resonance Raman excitation profiles. There is a general tendency for the experimental data points to be higher than the model's prediction with excitation at 266 (37,600 $cm^{-1}$), 250 (40,000 $cm^{-1}$), and 233 nm (43,000 $cm^{-1}$), suggesting some resonance with higher energy electronic transitions. Furthermore, for the weaker 789, 702, 1079, and 1158 $cm^{-1}$ peaks, the 290 nm data point appears much higher than predicted by the simulation, suggesting that the onset of preresonance may be changing the enhancement pattern or that a lower energy electronic transition may be resonant with these modes. On close examination of Figure 2, a slight deviation does appear between the experimental and simulated data ca. 35000 $cm^{-1}$, which may suggest a weak absorption band there. For both Thd and TMP, the resonance Raman excitation profiles and absorption spectra are fit reasonably well, with no significant deviations as was seen for 1-MeT. The error bars on the resonance Raman-derived parameters may seem small compared to the discrepancies between the experimental and simulated absorption spectra and resonance Raman excitation profiles, but these discrepancies yield relatively small changes in the excited-state parameters.

To better constrain the parameter set that accurately describes the absorption spectra and fundamental resonance Raman excitation profiles, the 1242 + 1376 $cm^{-1}$ combination band cross-section was measured at 260 nm for all three thymine derivatives (Table 4).

The UV resonance Raman spectra of all of the thymine derivatives exhibit similar relative intensity patterns for the most intense peaks. Even in 1-Met, the three most intense

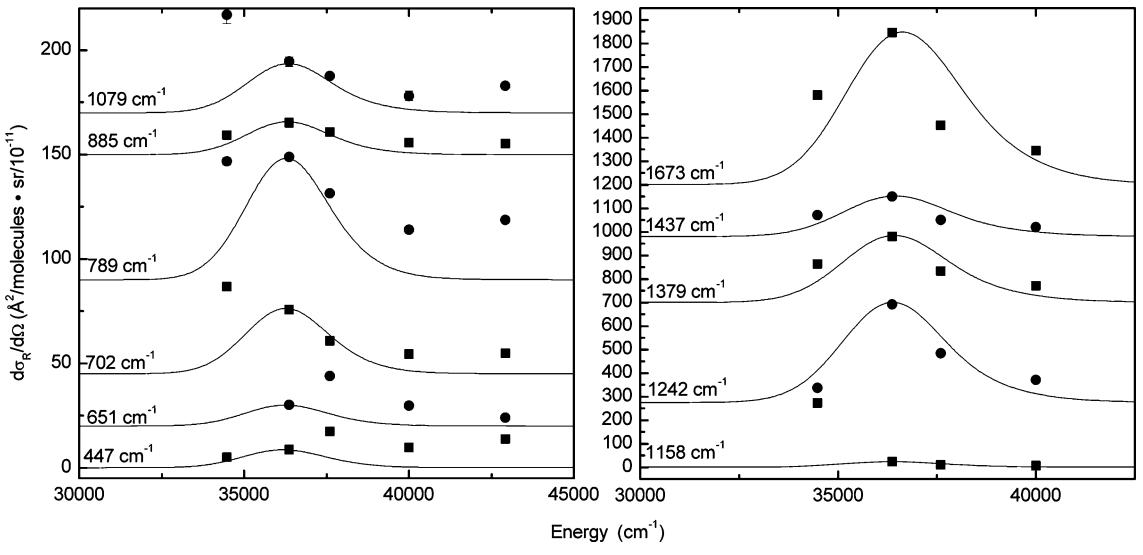


**Figure 3.** Experimental (points) and calculated (solid line) resonance Raman excitation profiles of 1-MeT. The excitation profiles were calculated with eq 1 with the parameters in Table 1. The excitation profiles have been offset along the ordinate for greater clarity of presentation.


dx.doi.org/10.1021/jp301952v | J. Phys. Chem. B 2012, 116, 10496−10503

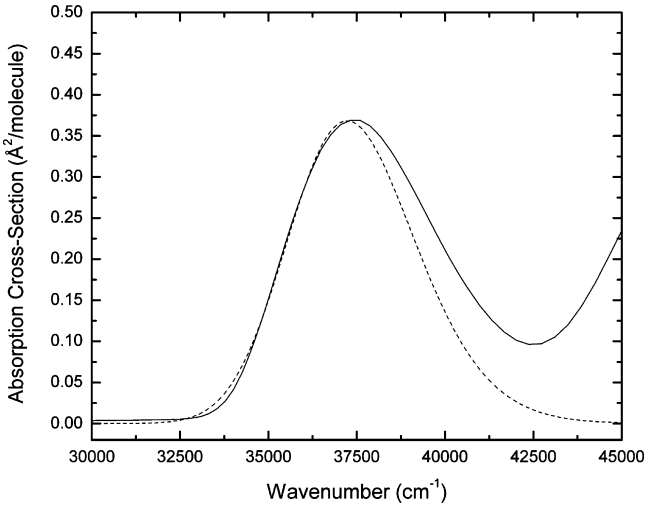


**Figure 4.** Experimental (solid line) and simulated (dotted line) absorption spectra of Thd. The simulated absorption spectrum was calculated using eq 2 with the parameters in Table 2. Discrepancies observed above 38 000 $cm^{-1}$ are due to higher energy electronic transitions, which were not modeled here.

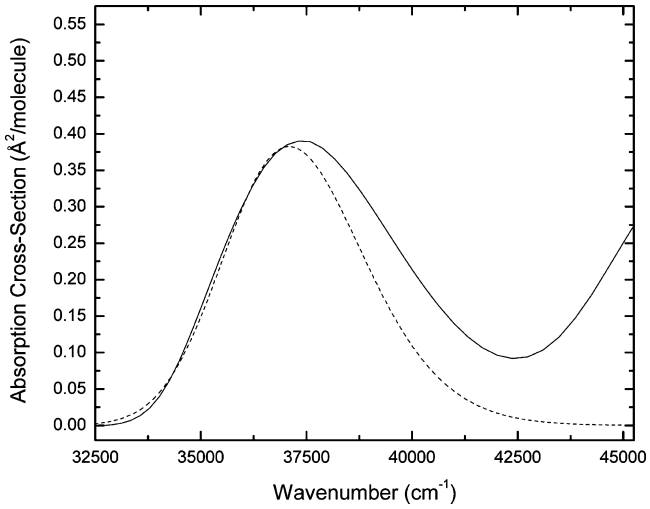


**Figure 6.** Experimental (solid line) and simulated (dotted line) absorption spectra of TMP. The simulated absorption spectrum was calculated using eq 2 with the parameters in Table 3. Discrepancies observed above 38000 $cm^{-1}$ are due to higher energy electronic transitions, which were not modeled here.

bands occur at the same wavenumber as in all the other thymine derivatives, including thymine itself. It is no surprise, then, that the excited-state structural displacements of the most intense bands are similar in these three derivatives to those in thymine for the same bands, and among the three derivatives. Similarly, the homogeneous line width, inhomogeneous line width, zero−zero energy, and transition length parameters are similar between thymine and the three derivatives, and among the three derivatives. For these parameters, however, some trends are observed as a function of the N1 substituent that will be discussed in more detail below.

## DISCUSSION

**Photochemical Structural Dynamics.** In understanding the photochemical structural dynamics of the thymine derivatives, it is helpful to first consider the photochemistry of thymine. Thymine preferentially forms the CPD with UVC irradiation, followed in yield by the [6−4] pyrimdine pyrimidinone photoproduct and trace amounts of the photohydrate.[2] Previous work[11,24,25] has shown that the excited-state structural dynamics that yield these photoproducts, particularly the partitioning of the dynamics among bond-lengthening and pyramidalization coordinates, appear to be correlated with substituent mass at the C5 position. The purpose of this study is to explore the correlation, if any, between N1 substituent mass and excited-state structural dynamics.

Considering the above photochemistry and that the resonance Raman intensity is roughly proportional[3,4] to $\Delta^2$, one can predict which vibrational modes will have resonance Raman intensity. This prediction assumes that the initial excited-state structural dynamics lie along the photochemical reaction coordinate. For the formation of either the photodimer or the photohydrate, there are two significant changes that occur during the photochemical reaction. One is that the C5═C6 double bond becomes a single bond. Therefore, one would expect to see high resonance Raman intensity for bands

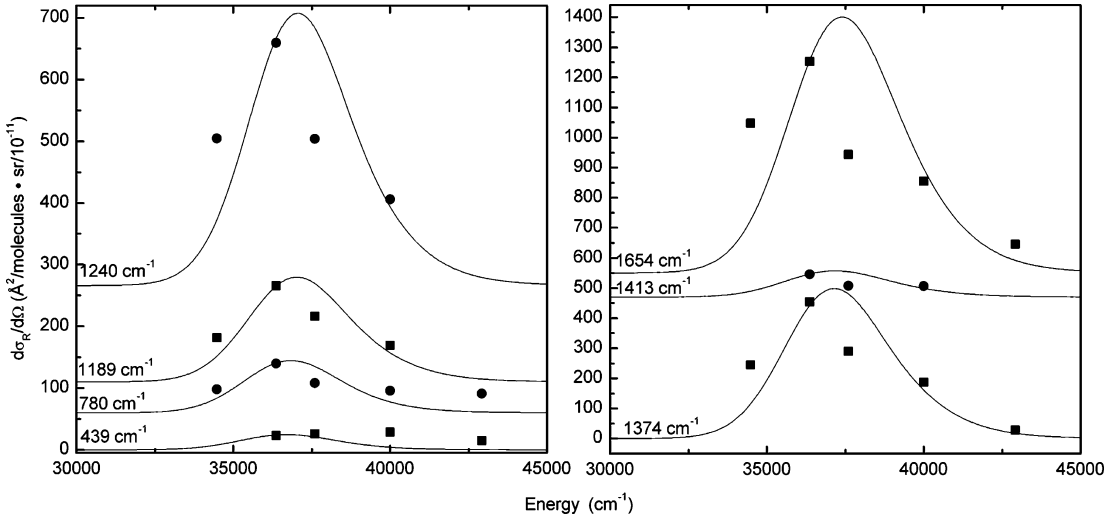


**Figure 5.** Experimental (points) and calculated (solid line) resonance Raman excitation profiles of Thd. The excitation profiles were calculated with eq 1 with the parameters in Table 2. The excitation profiles have been offset along the ordinate for greater clarity of presentation.


dx.doi.org/10.1021/jp301952v | J. Phys. Chem. B 2012, 116, 10496−10503

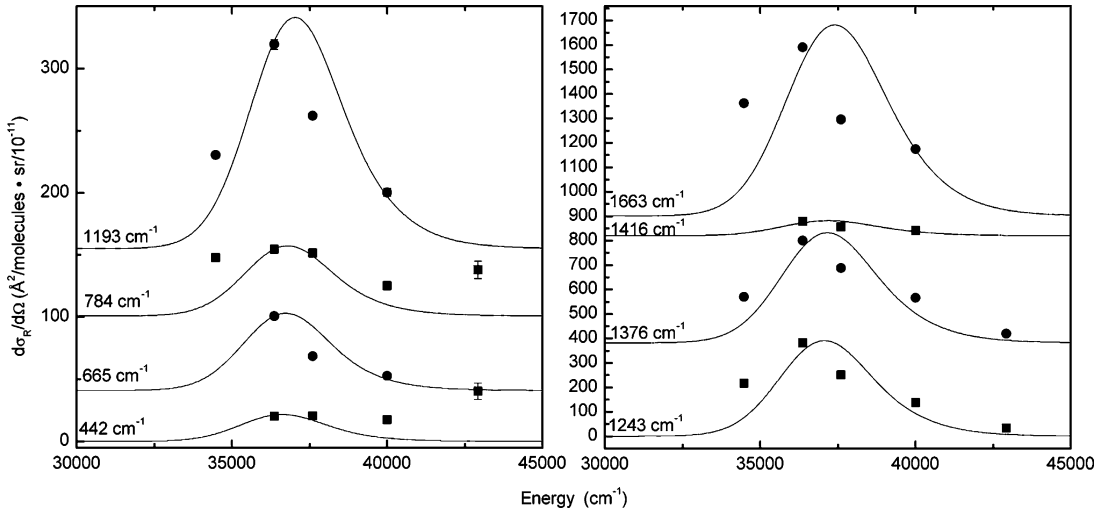


**Figure 7.** Experimental (points) and calculated (solid line) resonance Raman excitation profiles of TMP. The excitation profiles were calculated with eq 1 with the parameters in Table 3. The excitation profiles have been offset along the ordinate for greater clarity of presentation.

**Table 3. Raman Frequencies, Assignments, and Harmonic Parameters for TMP**

| mode[a] ($cm^{-1}$) | assignment[b] | $\|\Delta\|$[c] | $E$[d] ($cm^{-1}$) |
|---|---|---|---|
| 1663 | $\nu(C_5C_6)$ [61], be($C_6H$) [13], $\nu(C_6N1)$ [−8], $\nu(C_5Me)$ [−5] | 0.63 | 330.0 |
| 1416 | $\nu(C_2N_3)$ [15], $\nu(C_4C_5)$ [13], $CH_3$ umb [11], be($N_1H$) [9], $\nu(N_1C_2)$ [−8], be($C_4O$) [7], be($C_2O$) [7], ring $\delta$ 2 [−6], be($N_3H$) [−6] | 0.19 | 25.6 |
| 1376 | be($C_6H$) [42], $\nu(C_5C_6)$ [12], $\nu(N_1C_2)$ [9], $\nu(C_2N_3)$ [−9] | 0.52 | 186.0 |
| 1243 | $\nu(C_5Me)$ [29], $\nu(C_6N1)$ [−21], ring $\delta$ 1 [12], $\nu(N_1C_2)$ [10], $\nu(C_4C_5)$ [−10], $\nu(C_2N_3)$ [−8] | 0.51 | 161.7 |
| 1193 | $\nu(C_2N_3)$ [21], be($C_6H_{12}$) [20], be($N_1H_7$) [−16], $\nu(N_3C_4)$ [−12], $\nu(C_6N_1)$ [−11] | 0.36 | 77.3 |
| 784 | $\gamma(C_2O_8)$ [60], ring $\delta$ 6 [−12], ring $\delta$ 4 [8], $\gamma(C_4O_{10})$ [6], $\gamma(N_3H_9)$ [−5] | 0.26 | 26.5 |
| 665 | $\gamma(N_3H)$ [79], ring $\delta$ 4 [10] | 0.31 | 32.0 |
| 442 | ring $\delta$ 6 [32], $\gamma(N_1H)$ [−17], $\gamma(C_5H)$ [−17], ring $\delta$ 4 [16], ring $\delta$ 5 [−9], $\gamma(C_4O)$ [−7] | 0.26 | 14.9 |

[a]Frequencies listed are the experimental frequencies reported here. [b]Abbreviations: $\nu$ is stretching, $\delta$ is deformation, $\gamma$ is out-of-plane bending, and be is in-plane bending. The numbers represent the percentage of that internal coordinate in the mode. Assignments are from ref 8. Only the internal coordinates with percentages of 5% or larger are listed. [c]Displacements ($\Delta$) are in units of dimensionless normal coordinates and were obtained by fitting eqs 1 and 2 with the following parameters: temperature $T$ = 298 K, Brownian oscillator line shape $\kappa = \Lambda/D$ = 0.1, Gaussian homogeneous line width $\Gamma_G$ = 1260 $cm^{-1}$, inhomogeneous line width $\Theta$ = 1200 $cm^{-1}$, zero−zero energy $E_o$ = 35755 $cm^{-1}$ and transition length $M$ = 0.775 Å. The estimated errors in the parameters used in the calculation are as follows: $E_o$ ± 1%, $M$ ± 1%, $\Gamma$ ± 5%, $\Theta$ ± 5%, and $\Delta$ ± 5%. [d]$E$ is the reorganization energy calculated using $E = \Delta^2\omega/2$.

**Table 4. Experimental and Calculated Absolute Resonance Raman Combination Band Cross Sections for 1-Met, Thd, and TMP[a]**

| | experimental $d\sigma_R/d\Omega$ (Å$^2$/molecule × sr/$10^{-11}$) | calculated $d\sigma_R/d\Omega$ (Å$^2$/molecule × sr/$10^{-11}$) |
|---|---|---|
| 1-Met | 49 ± 0.1 | 49 |
| Thd | 127 ± 24 | 120 |
| TMP | 89 ± 21 | 88 |

[a]The excitation wavelength is 260 nm and the cross sections are given for the 1242 + 1376 $cm^{-1}$ combination band. Cross sections were calculated with eq 1 by using the parameters of Tables 1−3.

involving the C=C stretch. Also, the hybridization of the C5 and C6 carbons goes from $sp^2$ to $sp^3$. Therefore, modes involving either CH or CMe bending, deformation, or wagging on those carbons would be expected to have significant intensity. These structural dynamics are consistent with those of the thymine nucleobase and consistent with some computational and theoretical work.[11]

Comparing the thymine,[24] 1-Met, Thd, and TMP excited-state structural displacements, we can see that the three most intense bands are the ca. 1660, 1376, and 1240 $cm^{-1}$ modes, corresponding to the C5=C6 stretch, either C6H or N3H bend, and a ring stretch. For all the derivatives except 1-MeT, the excited-state structural dynamics appear to be similar, with most of the structural dynamics occurring along the C5=C6 bond-lengthening coordinate, with smaller, but significant distortion along the pyramidalization coordinate combined with general ring relaxation. In 1-MeT, the C5=C6 bond lengthening is still the major structural change, but general ring relaxation has increased, there is little C6H bending, and N3H bending appears as a significant structural dynamic. We attribute these differences in 1-MeT initial excited-state structural dynamics to greater coupling of the N1-methyl group into the vibrations of the thymine nucleobase, due to its intermediate mass between that of a proton and a sugar.

It must be mentioned that the resonance Raman intensities only probe the potential energy surface slopes at or very near to the Franck−Condon region before intra- and intermolecular dephasing mechanisms destroy the wavepacket overlaps in eqs 1 and 2. Therefore, only the *initial* excited-state structural dynamics can be measured. These initial excited-state structural dynamics do not provide much detail on later processes, such as internal conversion and intersystem crossing mechanisms and rates. Although the CPD mechanism has been alternatively described as either a singlet or triplet mechanism,[22,23] the resonance Raman-derived initial excited-state structural dynamics do not provide any resolution to this question.

**Broadening.** The homogeneous line width for nucleic acid derivatives has been typically considered to be due to solvent-induced dephasing.[24−27,36] Comparing the homogeneous linewidths obtained here for the various thymine derivatives


dx.doi.org/10.1021/jp301952v | J. Phys. Chem. B 2012, 116, 10496−10503

demonstrates that the line width increases from 900 $cm^{-1}$ for 1-MeT to 1260 $cm^{-1}$ for TMP. These values compare to 355 $cm^{-1}$ for thymine;[24] the change in homogeneous line width is significant between thymine and 1-MeT. These results indicate that the homogeneous line width increases with increasing size of the N1 substituent. This pattern suggests one of two models: either the solvent-induced dephasing increases with increasing size of the N1 substituent and/or the additional vibrational modes of the N1 substituent introduce another significant dephasing mechanism.

As the N1 substituent increases from a methyl group to a deoxyribose to a deoxyribose monophosphate, the number of sites of interaction between the solvent and solute increase substantially. Similarly, changes in the N1 substituent may affect the local solvation structure proximal to C5═C6, the chromophoric site, and affect the excited-state dephasing mechanism and/or line width. Interestingly, the homogeneous line width increases the most between thymine and 1-MeT, suggesting that proximal effects may be the most significant factor, arguing for the second factor above as being the most significant.

It has been established before[3] that unenhanced Raman vibrations may still lead to increased homogeneous broadening. One mechanism is that modes with no displacement or excited-state frequency changes may still be susceptible to solvent effects, which induce broadening and dephasing of the excited-state wavepacket and lead to an effective homogeneous line width. Another mechanism is that low frequency modes may still have very large excited-state slopes and experience significant dynamics. If those dynamics occur significantly faster than the vibrational period, the Raman amplitude in eq 1 may not reach a significant value, and these modes would not exhibit observable resonance Raman intensity. These "missing modes" have been implicated in the torsional dynamics of the trans−cis isomerization of bacteriorhodopsin.[3] Although this mechanism may be at work in thymine, it is difficult to identify any physically reasonable low-frequency mode,[8] which may undergo essentially barrierless dissociative dynamics in the excited-state such as may be expected in an isomerization reaction. There are some N−$CH_3$ torsional modes that are expected to appear at very low frequencies, based on DFT calculations,[8] which may also contribute to this additional dephasing. It would be instructive to measure the excited-state dephasing times as a function of solvent viscosity and other solvent parameters which may correlate with dephasing mechanisms.

The inhomogeneous component of the broadening is also quite large, but consistent with that measured previously in UV resonance Raman determinations of excited-state structural dynamics of nucleobases[11,24,25] and visual pigments.[40] The inhomogeneous component has been attributed to solvent−solute interactions, static on the dephasing time scale, that yield a distribution of electronic zero−zero energies in the ensemble of molecules being probed.[3,4,36,37] In the pyrimidine nucleobases, these interactions have been probed with visible Raman spectroscopy to identify those molecular frequencies that are particularly sensitive to solvent, with the N−H and C═C sites being the most interacting.[41] The larger inhomogeneous line width for the N-substituted thymine derivatives is consistent with the larger homogeneous line width in showing the greater solvent interaction on the dephasing time scale and longer.

## CONCLUSIONS

Good-quality UV resonance Raman spectra of the N1-substituted thymine derivatives 1-Met, Thd, and TMP demonstrate that the excited-state structural dynamics of Thd and TMP are similar to that of thymine. However, 1-MeT exhibits similar C5C6 bond lengthening, greater ring relaxation and N3H bending, and less C5 and C6 pyramidalization than thymine.

## AUTHOR INFORMATION


### Corresponding Author

*E-mail: glen.loppnow@ualberta.ca.

### Present Addresses

[†]Canadian Light Source Inc., University of Saskachewan, 101 Perimeter Road, Saskatton, SK S7N 0X4

[‡]CanmetENERGY, 1 Oil Patch Drive, Devon, AB T9G 1A9


### Notes

The authors declare no competing financial interest.

## REFERENCES


(1) Lehninger, A. L. *Biochemistry*; Worth Publishers, Inc.: New York, 1975; Vol 2, p 309−333.

(2) Ruzsicska, B. P.; Lemaire, D. G. E. In *CRC Handbook of Organic Photochemistry and Photobiology*; Horspool, W. H., Song, P.-S., Eds.; CRC Press: New York, 1995; pp 1289−1317.

(3) Myers, A. B.; Mathies, R. A. Biological Applications of Raman Spectroscopy. In *Resonance Raman Spectra of Polyenes and Aromatics*; Spiro, T. G., Ed.; Wiley-Interscience: New York, 1987; Vol.2, pp 1−58.

(4) Myers, A. B. Excited Electronic State Properties From Ground-State Resonance Raman Intensities. In *Laser Techniques in Chemistry*; Myers, A. B., Rizzo, T. R., Eds.; Wiley: New York, 1995; pp 325−384.

(5) Lagant, P.; Vergoten, G.; Efremov, R.; Peticolas, W. L. *Spectrochim. Acta A* **1994**, *50*, 961−971.

(6) Rush, T.; Peticolas, W. L. *J. Phys. Chem.* **1995**, *99*, 14647−14658.

(7) Aida, M.; Kaneko, M.; Dupuis, M.; Ueda, T.; Ushizawa, K.; Ito, G.; Kumakura, A.; Tsuboi, M. *Spectrochim. Acta A* **1997**, *53*, 393−407.

(8) Yarasi, S.; Billinghurst, B. E.; Loppnow, G. R. *J. Raman Spectrosc.* **2007**, *38*, 1117−1126.

(9) Peticolas, W. L.; Rush, T. *J. Comput. Chem.* **1995**, *16*, 1261−1270.

(10) Lagant, P.; Vergoten, G.; Peticolas, W. L. *J. Raman Spectrosc.* **1999**, *30*, 1001−1007.

(11) Billinghurst, B. E.; Oladepo, S. A.; Loppnow, G. R. In *Radiation Induced Molecular Phenomena in Nucleic Acidserer*; Shukla, M. K., Leszczynski, J., Eds.; Springer-Verlag: Dordrecht, The Netherlands, 2008, pp 237−263.

(12) Fodor, S. P. A.; Rava, R. P.; Hays, T. R.; Spiro, T. G. *J. Am. Chem. Soc.* **1985**, *107*, 1520−1529.

(13) Zhu, X.-M.; Wang, H.-G.; Zheng, X.; Phillips, D. L. *J. Phys. Chem. B* **2008**, *112*, 15826−15836.

(14) Pecourt, J.-M. L; Peon, J.; Kohler, B. *J. Am. Chem. Soc.* **2000**, *122*, 9348−9349.

(15) Nikogosyan, D. N.; Angelov, D.; Soep, B.; Lindqvist, L. *Chem. Phys. Lett.* **1996**, *252*, 322−326.

(16) Reuther, A.; Nikogosyan, D. N.; Laubereau, A. *J. Phys. Chem.* **1996**, *100*, 5570−5577.

(17) Reuther, A.; Iglev, H.; Laenen, R.; Laubereau, A. *Chem. Phys. Lett.* **2000**, *325*, 360−368.

(18) Pecourt, J.-M. L.; Peon, J.; Kohler, B. *J. Am. Chem. Soc.* **2001**, *123*, 10370−10378.

(19) Gustavsson, T.; Sharonov, A.; Markovitsi, D. *Chem. Phys. Lett.* **2002**, *351*, 195−200.

(20) Hare, P. M.; Crespo-Hernandez, C. E.; Kohler, B. *Proc. Natl. Acad. Sci. U.S.A.* **2007**, *104*, 435−440.

(21) Hare, P. M.; Crespo-Hernandez, C. E.; Kohler, B. *J. Phys. Chem. B* **2006**, *110*, 18641−18650.

(22) Kwok, W.-M.; Ma, C.; Phillips, D. L. *J. Am. Chem. Soc.* **2008**, *130*, 5131−5139.

(23) Schreier, W. J.; Kubon, J.; Regner, N.; Haiser, K.; Schrader, T. E.; Zinth, W.; Clivio, P.; Gilch, P. *J. Am. Chem. Soc.* **2009**, *131*, 5038−5039.

(24) Yarasi, S.; Brost, P.; Loppnow, G. R. *J. Phys. Chem. A* **2007**, *111*, 5130−5135.
(25) Yarasi, S.; Ng, S.; Loppnow, G. R. *J. Phys. Chem. B* **2009**, *113*, 14336−14342.
(26) Billinghurst, B. E.; Yeung, R.; Loppnow, G. R. *J. Phys. Chem. A* **2006**, *110*, 6185−91.
(27) Ng, S. S.; Teimoory, F.; Loppnow, G. R. *J. Phys. Chem. Lett.* **2011**, *2*, 2362−2365.
(28) Schreier, W. J.; Schrader, T. E.; Koller, F. O.; Gilch, P.; Crespo-Hernandez, C. E.; Swaminathan, V. N.; Carell, T.; Zinth, W.; Kohler, B. *Science* **2007**, *315*, 625−629.
(29) Durbeej, B.; Eriksson, L. A. *J. Photochem. Photobiol. A* **2002**, *152*, 95−101.
(30) Webb, M. A.; Fraga, E.; Loppnow, G. R. *J. Phys. Chem.* **1996**, *100*, 3278−3287.
(31) Mathies, R.; Oseroff, A. R.; Stryer, L. *Proc. Natl. Acad. Sci. U.S.A.* **1976**, *73*, 1−5.
(32) Loppnow, G. R.; Fraga, E. *J. Am. Chem. Soc.* **1997**, *119*, 895−905.
(33) Webb, M. A.; Kwong, C. M.; Loppnow, G. R. *J. Phys. Chem. B* **1997**, *101*, 5062−5069.
(34) Fraga, E.; Loppnow, G. R. *J. Phys. Chem. B* **1998**, *102*, 7659−7665.
(35) Lee, S.-Y.; Heller, E. J. *J. Chem. Phys.* **1979**, *71*, 4777−4788.
(36) Mukamel, S. *Principles of Nonlinear Optical Spectroscopy*; Oxford University Press: New York, 1995.
(37) Li, B; Johnson, A. E.; Mukamel, S.; Myers, A. B. *J. Am. Chem. Soc.* **1994**, *116*, 11039−11047.
(38) Shoute, L. C. T.; Loppnow, G. R. *J. Chem. Phys.* **2002**, *117*, 842−850.
(39) Morzyk-Ociepa, B.; Nowak, M. J.; Michalska, D. *Spectrochim. Acta A* **2004**, *60*, 2113−2123.
(40) Loppnow, G. R.; Mathies, R. A. *Biophys. J.* **1988**, *54*, 35−43.
(41) Beyere, L.; Arboleda, P.; Monga, V.; Loppnow, G. R. *Can. J. Chem.* **2004**, *82*, 1092−1101.